

1 Integrated Geophysical Analysis of Rangpur Saddle: Insights on Tectonics and 2 Magnetic Mineral Potential of North-Western Bangladesh

3
4 Mohammad Tawhidur Rahman Tushar¹, Asif Ashraf², Md. Mahfuz Alam¹, Md Nasif Jamil¹, Saba Karim¹,
5 Md. Shahjahan³, Md. Anwar Hossain Bhuiyan¹

6
7 ¹Department of Geology, University of Dhaka, Dhaka-1000, Bangladesh

8 ²Department of Earth Sciences, University of Oregon, Eugene, Oregon-97401, United States of America

9 ³Geological survey of Bangladesh, 153 Pioneer Road, Dhaka-1000, Bangladesh

10
11 *Correspondence to: Mohammad Tawhidur Rahman Tushar (mtrt@du.ac.bd) and Asif Ashraf (aashraf@uoregon.edu)*

12 13 Abstract

14
15 The northwestern region of Bangladesh holds untapped potential for magnetic mineral deposits at
16 shallow depths. Unlike much of Bangladesh, characterized by thick sediments of the Bengal Basin,
17 this area is an extension of the Indian Shield, often referred to as the Stable Platform. It is also
18 geologically distinct, hosting structures related to the breakup of Pangea. The geology and
19 tectonics of this region have remained largely understudied. To address this gap, this study
20 integrates gravity, magnetic, seismic, and drilling data to investigate the subsurface structure and
21 evaluate the resource potential of the area. We utilize advanced filtering and modeling techniques,
22 including tilt derivatives and horizontal gradient methods, to understand the tectonic framework
23 and geometry of the subsurface structures. Our spatial analysis, using multiple geophysical
24 datasets, reveals dipolar magnetic anomalies, which we attribute to gabbroic intrusions along
25 extensional faults that define the region's horst and graben structures. To validate our
26 interpretations, we developed an integrated 2-D subsurface model that aligns with the observed
27 geophysical data. However, the study is limited by the availability of high-resolution seismic data
28 and the sparse distribution of drilling locations, which may affect the precision of our subsurface
29 characterization. Our findings provide crucial insights into the tectonic evolution of the stable
30 platform and underscore the economic potential of the Rangpur Saddle, the shallowest part of the
31 stable platform, for mineral exploration. These insights pave the way for further exploration and
32 development initiatives focused on uncovering the mineral wealth of this underexplored region.

33 34 1. Introduction

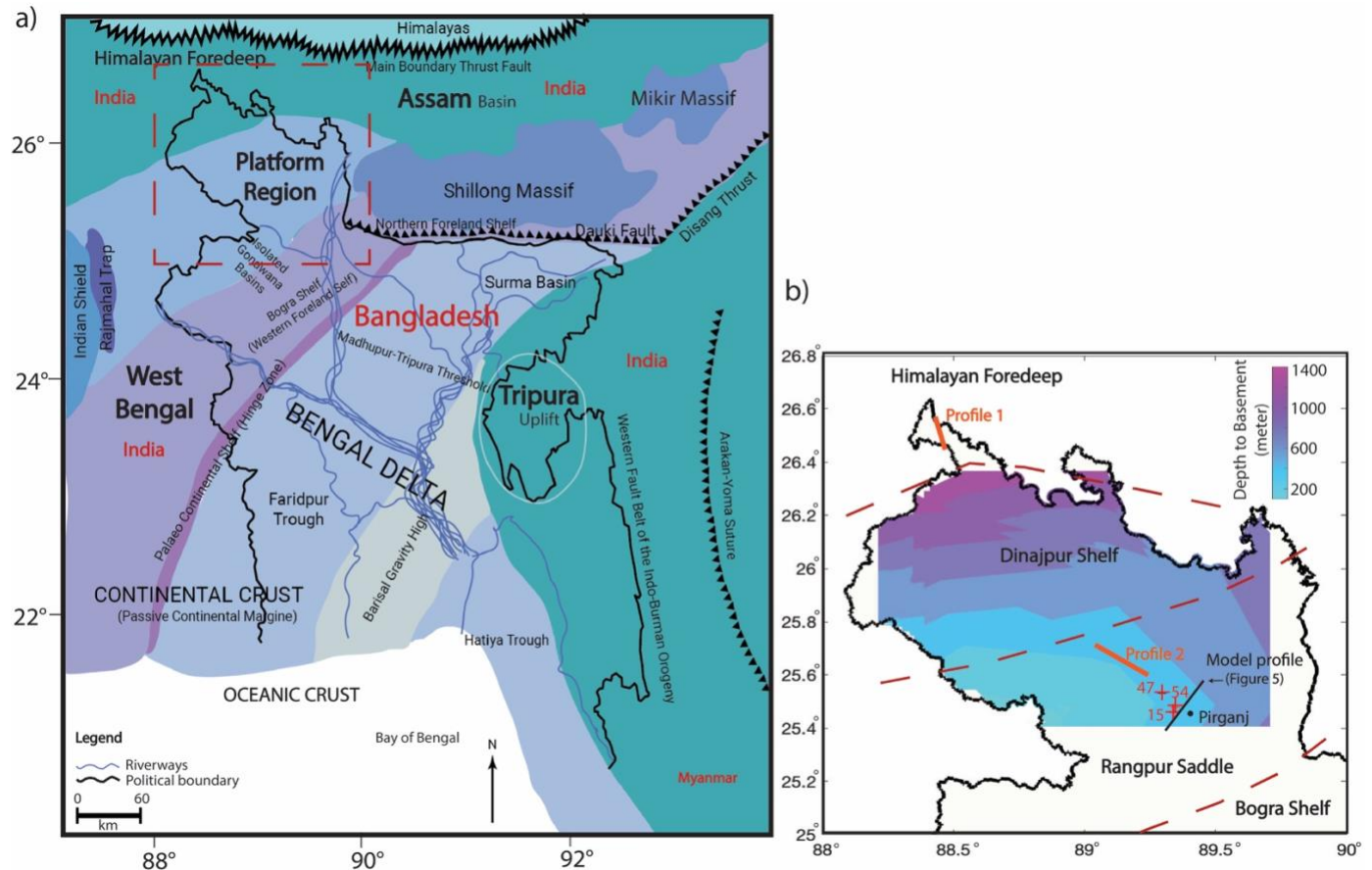
35
36 The northwestern part of Bangladesh is rich in potential mineral resources. The geological
37 diversity of this area suggests the presence of other valuable minerals that remain largely
38 unexplored (Akhtar, 2005; Hasan et al., 2023; Moon, 2022). In this area, basement rocks are
39 present at relatively shallow depths of 128 meters, hosting a spectrum of economic mineral
40 resources, including coal, limestone, white clay, and hard rock (Khan and Rahman, 1992).
41 Notably, Pirganj in the Rangpur district (**Figure 1**) records the country's highest magnetic
42 anomaly, suggesting the potential for magnetic mineral ore deposits. In the 1990s, drilling
43 activities were conducted in the region after developing a 2D subsurface model by the Geological
44 Survey of Bangladesh (GSB) in collaboration with the United States Geological Survey (USGS).
45 Despite these efforts, no noteworthy ore body was identified during the drilling process (Rahman

46 and Ullah, 2009). Moreover, the tectonic evolution of the Paleo-Proterozoic basement in the
47 northwest region of the Bengal Basin still needs to be studied.

48
49 The study area is located in a region commonly referred to as the Rangpur platform or saddle
50 (Masum et al., 2021), an eastern extension of the Indian Shield (Alam et al., 2003). The northern
51 part of the Rangpur Saddle rests on a shallow Precambrian basement, ranging from 130 to 1000
52 meters in depth. This area of Bangladesh is geologically stable, characterized predominantly by
53 horsts and grabens, which were formed during the Cretaceous rifting of the Indian plate from the
54 Antarctica-Australia section of Gondwanaland (Curry, 1991; Curry and Moore, 1974). Although
55 the basement primarily consists of diorite, tonalite, and granodiorite, it is also intersected by
56 pegmatite and mafic/ultramafic dykes (Hossain et al., 2007; Kabir et al., 2001).

57
58 In this study, we explore the possibility of mafic dykes as the source of high magnetic anomalies
59 using multiple geophysical datasets while establishing the regional geological structure of this
60 significantly understudied area. We aim to conduct integrated spatial analysis and develop
61 subsurface models with gravity, magnetic, seismic, and drilling data to understand the regional
62 geological features. Gravity and magnetic data are widely used to understand and characterize
63 geological formations, particularly for identifying thin magnetic layers or faults (Adebiyi et al.,
64 2023; Jaffal et al., 2010). High-resolution potential field data help identify structures related to
65 local-scale mineralization that are covered by shallow alluvium or other unconsolidated sediments
66 (Hendrickson, 2016; McCafferty et al., 2014). Since potential field data can yield multiple
67 solutions (Filina et al., 2019), we also incorporate seismic and drilling data to constrain the
68 subsurface framework and produce more reliable results (Sundararajan, 2012). Our study applies
69 various filters to magnetic and gravity data to enhance and delineate regional crustal structures,
70 with a focus on highlighting structure edges where metallic mineral deposits are likely to be found
71 (Hildenbrand, 2000).

72



73
 74 Figure 1: (a) Regional geological map of Bangladesh adopted from Hossain et al. (2019), illustrating various
 75 geological and tectonic zones with distinct color coding. The names of neighboring countries are labeled in red. The
 76 red dashed box indicates the study area in the northwestern part of Bangladesh. (b) The map of the northwestern
 77 Bangladesh region shows basement depth with its tectonic subdivisions. Regional basement depths are collected from
 78 GSB and constructed from various seismic reflection surveys. Red dashed lines mark the approximate boundaries of
 79 the tectonic divisions. Seismic profiles (orange lines) and drilling locations (red plus signs) utilized in this study are
 80 also highlighted. Our specific study area, Pirganj, is also shown on the map, where the highest magnetic anomaly is
 81 observed. The integrated 2-D modeling profile of this study is also shown in this map with a solid black line.

82
 83 **2. Geological setting**

84
 85 Bangladesh, though geographically compact, possesses a complex and diverse geological
 86 framework shaped largely by its position within the Bengal Basin (Roy and Chatterjee, 2015). This
 87 region is primarily divided into two major tectonic units (Morgan and McIntire, 1959). To the
 88 northwest of the hinge zone (see **Figure 1a** for location), the stable platform region features a
 89 shallow basement composed predominantly of Precambrian-aged rocks (Uddin and Lundberg,
 90 1998). Conversely, the southeastern portion of the Bengal Basin comprises a geosynclinal basin,
 91 distinguished by significant sediment accumulation, with sediment thicknesses exceeding 12
 92 kilometers (Alam, 1989). This tectonic configuration highlights the geological contrasts between
 93 the stable platform and the more dynamic, subsiding basin to the southeast.

94
 95 The Bengal Basin, encompassing Bangladesh and parts of the neighboring Indian states of West
 96 Bengal, Assam, and Tripura, is situated at the northeastern edge of the Indian craton. It is one of

97 South Asia's largest peripheral collisional foreland basins, with a sedimentary sequence spanning
98 from the Early Cretaceous to the Holocene (DeCelles, 2011). The study area, located in the
99 northwest part of the basin and known as the stable platform, consists of three geological
100 components (Hossain et al., 2019): the Dinajpur Shelf, Rangpur Saddle, and the Bogra Shelf
101 (**Figure 1b**). The Himalayan Foredeep region, located just north of the Dinajpur Shelf, contains
102 the deepest basement in the stable platform (**Figure 1b**) and hosts numerous faults associated with
103 extensional tectonics (**Figure 2a**). South of the Foredeep region, the Dinajpur Shelf gently slopes
104 northward toward the Himalayan Foredeep at an angle of 1-3 degrees and is covered by recent
105 sedimentary deposits. The Rangpur Saddle, the southern block of the Dinajpur Shelf, connects the
106 Indian Shield to the Shillong Plateau and contains the shallowest basement in the Bengal Basin
107 (Jain et al., 2020) (**Figure 1b**). The Bogra Shelf, on the southern slope of the Rangpur Saddle, was
108 formed during the Early Cretaceous rifting of the Indian plate from Gondwana (Alam, 1989; Alam
109 et al., 2003). Both the Rangpur Saddle and Bogra Shelf host several horsts and graben, and half-
110 graben basins (**Figure 2b**).

111
112 The entire northwestern Bangladesh is geologically stable with minimal folding impact that can
113 be traced back to Rodinia and Nuna or Columbia supercontinents (Ameen et al., 2007; Zhang et
114 al., 2012). Ameen et al. (2007) suggest that the basement is a separate micro-continental fragment
115 trapped during the northward migration of the Indian Plate, while Hossain et al. (2007) propose
116 that it is a continuation of the central Indian tectonic zone. During the Precambrian, only the stable
117 shelf of the Bengal basin was part of the Indian Plate within Gondwana. By the Middle Jurassic
118 (~170–175 Ma), the Indian Plate began drifting and became isolated by the end of the Paleocene
119 (~55.9 Ma) (Hossain et al., 2019). During the Late Paleozoic–Mid Mesozoic, the stable shelf was
120 developed as an intra-cratonic rift basin with Gondwana sediments in graben structures, followed
121 by Kerguelen igneous activity and widespread Rajmahal Trap volcanism (Hossain et al., 2019;
122 Valdiya, 2016).

123
124 The basement in our study area is the shallowest part of the Stable Shelf, which is uplifted to a
125 depth of 128 m from the surface, overlain by the Plio-Pleistocene Dupi Tila Sandstone and
126 Madhupur Clay, and is mainly composed of crystalline rocks, including granite, granodiorite, and
127 gneiss (Alam et al., 2003; Hossain et al., 2007). There is no outcrop of Precambrian basement in
128 this area, and the commonly observed horst and graben structures control the stratigraphic
129 subdivision. The Precambrian basement in this region lies beneath thick Cenozoic clastic deposits
130 and is primarily felsic in composition, intersected by mafic-ultramafic and occasional felsic dykes
131 (Chowdhury et al., 2022). Fault-bound graben basins within the basement contain Carboniferous
132 rock units from the Permian Period (286 to 245 million years ago) called the Gondwana formation,
133 marking the oldest sedimentary rocks in Bangladesh (Alam et al., 2003; Jain et al., 2020). Above
134 the Permian Gondwana formation is the Jurassic Rajmahal Trap Formation, consisting of volcanic
135 basalt strata (Alam, 1989; Roy and Chatterjee, 2015). The Shibganj Trapwash Formation overlays
136 it, formed through weathering and erosion of the underlying igneous rocks (Khan, 1991).

137
138 The Rangpur Saddle serves as the subsurface extension of the Indian shield, stretching between
139 the Shillong Plateau to the east and the Rajmahal Hills to the west. Geophysical studies have
140 identified two major faults framing the Garo-Rajmahal gap: the Dhubri-Jamuna Fault (western
141 edge of Garo Hills) and the Rajmahal Fault (eastern edge of Rajmahal Hills), which encloses the
142 Rangpur saddle (Hossain et al., 2019). Tectonic activities, particularly extensional tectonics during

143 continental rifting, have significantly disrupted the basement topography, forming numerous
 144 horsts and grabens (Ahamed et al., 2020; Khan and Rahman, 1992). Despite this, the study area
 145 remains predominantly flat with sediment covers (Khan, 1991) from the Pleistocene to the
 146 Holocene period (Reimann and Hiller, 1993). Near the Rangpur Saddle, the eastern part of the
 147 Indian Shield includes three major tectonic domains: Singhbhum Craton, Singhbhum Mobile Belt,
 148 and Chhotanagpur Gneissic Complex (Mukhopadhyay and Matin, 2020). Singhbhum Craton is
 149 characterized by prolonged crustal evolution during the Archean, comprising lithologies such as
 150 granitoids and metamorphic rocks. Singhbhum Mobile Belt underwent accretion and modification
 151 through volcanics, dyke swarms, and various intrusive bodies in the Proterozoic. Chhotanagpur
 152 Gneissic Complex comprises mainly of gneisses, amphibolites, and granulites with mafic dyke
 153 swarms, forming a structurally complex mobile belt. The tectonics of this region can be
 154 characterized by intra-cratonic structural depressions between the uplifted tectonic blocks. Seismic
 155 reflection studies indicate that the Moho in this region is complex and laminated, suggesting a
 156 history of tectonic and magmatic activity (Valdiya, 2016). In the West Bengal basin, the Moho is
 157 relatively shallow and horizontal (at a depth of 36 km), while other nearby regions (e.g., Kutch
 158 basin) have a dipping Moho influenced by tectonic processes (Rangin and Sibuet, 2017).

159
 160 Magnetic minerals, particularly iron ore, are widely found across the Indian Shield. These iron
 161 deposits typically appear as metamorphosed banded iron or silica formations. In eastern India, the
 162 Precambrian iron ore of the Singhbhum-North Orissa region is a horseshoe-shaped synclinorium
 163 that contains the most significant iron deposits near Bangladesh. The first discovery of iron ore in
 164 Bangladesh is located on the Dinajpur slope of the Rangpur platform (Alam et al., 2003). Around
 165 30 km southwest of our study area, Masum et al. (2021) report iron ore-bearing basement rock
 166 about 30 km southwest of our study area, with the iron ores occurring as a thin, metamorphosed
 167 laminated layer.

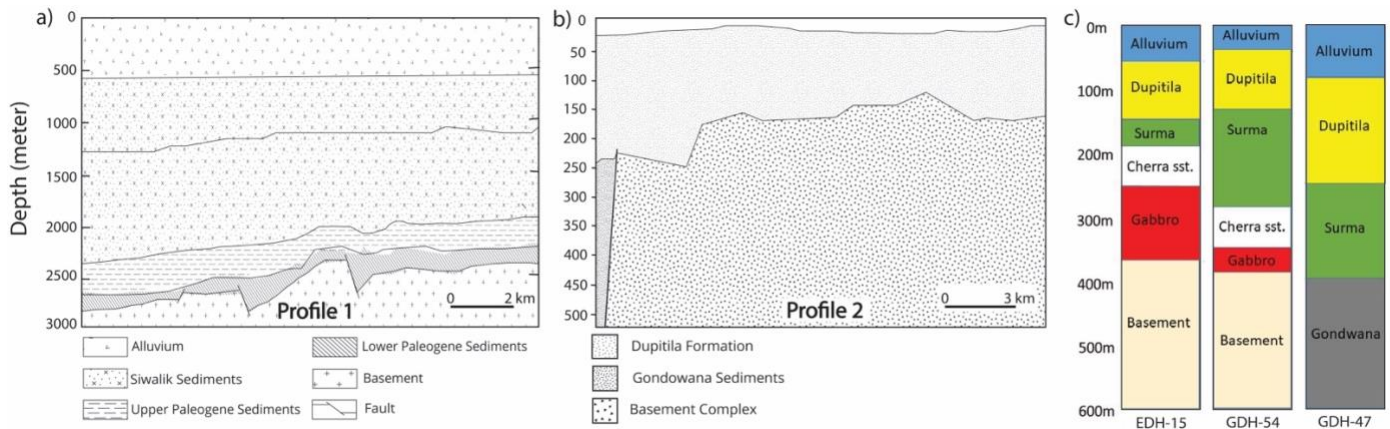
168
 169 To understand the geological succession in Pirganj and its surroundings, we present a generalized
 170 lithological depiction using data from EDH-15 and GDH-54 drill holes (Table 1).

171
 172 Table 1: Stratigraphic Succession of Pirganj and its adjoining Areas according to drill holes EDH-15 and GDH-54
 173

Age	Rock Units	Lithology	Thickness (m)
Recent	Alluvium	Loose sand, medium to coarse-grained	52
Unconformity			
Pliocene	Dupitila	Sandstone (SST), silty SST, pebbly SST, pebbly bed; SST: medium to coarse-grained, pebbles: quartzite, gneiss and schist	33
Unconformity			
Late Oligocene to Early Miocene	Surma	Alteration of SST and shales and their combination, sand and silty shale. SST: fine to medium-grained; shale: soft and sticky	125
Unconformity			

Late Cretaceous to Paleocene	Cherra Sandstone	Sandstone: medium to coarse-grained	50
Unconformity			
	Basement	Gabbro; Diorite, quartz diorite, granodiorite, quartz monazite.	180+ (base not seen)

174
175



176
177
178
179
180
181
182

Figure 2: Interpretation of seismic and drilling data used for integrated geophysical analysis in this study. (a) and (b) present interpretations of the two seismic profiles analyzed. (c) shows the drilling log data, which correlates with the 2D subsurface models and assists in spatial analysis. Refer to Figure 1b for their locations. Seismic profile 1 is from Himalayan Foredeep region while profile 2 represents Rangpur Saddle. All the drilling logs are situated near the highest observed magnetic anomaly in Pirganj, located in Northwestern Bangladesh.

183 3. Data and Methodology

184 3.1 Geophysical Data

185
186
187 In this study, we apply an integrative analytical approach utilizing multiple geophysical datasets
188 for spatial analysis and 2-D subsurface modeling. Our primary datasets are potential field data,
189 specifically gravity and magnetic data, provided by the Geological Survey of Bangladesh (GSB).
190 We use Bouguer gravity data and total magnetic intensity data for our analysis.

191
192 The gravity data presented in this paper represent a cumulative dataset acquired through successive
193 land-based surveys initiated in the late 1970s and continuing to the present day. These surveys
194 were primarily conducted during the dry season (November–April) to ensure accessibility,
195 gradually covering approximately 8,000 km² in northwestern Bangladesh. Data acquisition
196 methodology evolved over the decades to incorporate technological advancements. During the
197 earlier campaigns (starting in the 1970s), gravity measurements were taken using an analog Sodin
198 Worden gravimeter (Model WS 410), while surveys conducted after 2007 also deployed the digital
199 Scintrex CG-5 AutoGrav. Cross-verification between the analog and digital instruments was
200 performed regularly in later phases to ensure consistency across the historical dataset. Similarly,
201 positioning methods were modernized over time; while earlier observation points relied on
202 standard benchmarks from the Survey of Bangladesh, later campaigns utilized handheld GPS
203 receivers and the CG-5’s integrated GPS for precise coordinate determination.

204 Throughout the survey history, observation points were generally spaced 1–1.5 km apart.
205 Elevations were determined using digital leveling referenced to benchmarks from the Survey of
206 Bangladesh, maintaining high vertical accuracy crucial for gravity corrections. The Sylhet Gravity
207 Base Station, connected to the IGSN 71 network, served as the primary national reference, with
208 local sub-bases established to correct for instrument drift. Standard geophysical corrections—
209 including those for instrumental drift, tidal and latitude variations, and elevation differences—
210 were applied to the entire dataset. Bouguer corrections were calculated using a crustal density of
211 2.0 kg/m³.

212
213 Between 1979 and 1980, Hunting Geology & Geophysics Ltd. completed a nationwide
214 aeromagnetic survey for the Government of Bangladesh, under the auspices of the Geological
215 Survey of Bangladesh and Petrobangla. Flying a Geometrics G-803 proton magnetometer just 500
216 ft (\approx 152 m) above ground, the crew collected total-field data along flight lines oriented N 45° W
217 on a nominal 3 km grid (locally tightened to 1 km) and crossed them with tie-lines oriented N 45°
218 E at 5 km spacing. Measurements were recorded every two seconds with a resolution of \pm 0.05 nT,
219 within a regional field that varied from 44 848 nT to 47 086 nT (inclinations 28° 30'–38° 30',
220 declinations 13° W–37° W). All readings were archived in both digital and analogue form, and the
221 data were uniformly shifted upward by 900 nT so that every value is positive.

222
223 The topography data used in our geophysical modelling (**Figure S1**) are obtained from the online
224 repository of the Scripps Institution of Oceanography, which are derived from satellite altimetry
225 (Smith and Sandwell, 1997). Additionally, we incorporate interpretations of seismic images
226 obtained from GSB to correlate our findings from gravity and magnetic data. However, raw
227 seismic images are unavailable, as private entities originally collected them. To further refine our
228 2-D integrated modeling, we use drilling data from three boreholes near our study area, also
229 provided by GSB (see **Figure 1b** for the locations).

230

231 **3.2 Methods**

232
233 For geophysical spatial analysis, we use gravity and magnetic anomaly maps. The Bouguer gravity
234 anomaly data are provided by GSB. For the total magnetic intensity map, we apply a differential
235 reduction to the pole (RTP) to adjust the magnetic grid (Arkani-Hamed, 2007). This correction
236 involves computing magnetic inclination, declination, and total magnetic field values based on the
237 International Geomagnetic Reference Field (Alken et al., 2021) with a magnetic epoch of 1980.

238
239 The next step in our spatial analysis methodology involves removing the regional trend from both
240 the gravity and magnetic data. This process, known as regional-residual separation, is essential for
241 isolating local anomalies by filtering out the broader, long-wavelength trends associated with
242 large-scale geological structures (Ashraf and Filina, 2023b; Kheyrollahi et al., 2021; Núñez-
243 Demarco et al., 2023). Total magnetic intensity anomalies arise from the combined effect of
244 induced and remanent magnetization in rocks. Induced magnetization is caused by the Earth's
245 ambient field acting on magnetic minerals, so it is aligned parallel to the present field, whereas
246 remanent magnetization is a permanent magnetization inherent to the rocks (acquired in the past)
247 that often points in a different direction (reflecting the Earth's field at the time of rock formation).
248 The total magnetization is the vector sum of the induced and remanent contributions. As a result,
249 the direction and relative magnitude of each component strongly influence the observed anomaly.
250 If the induced and remanent magnetization vectors are aligned, they reinforce each other to

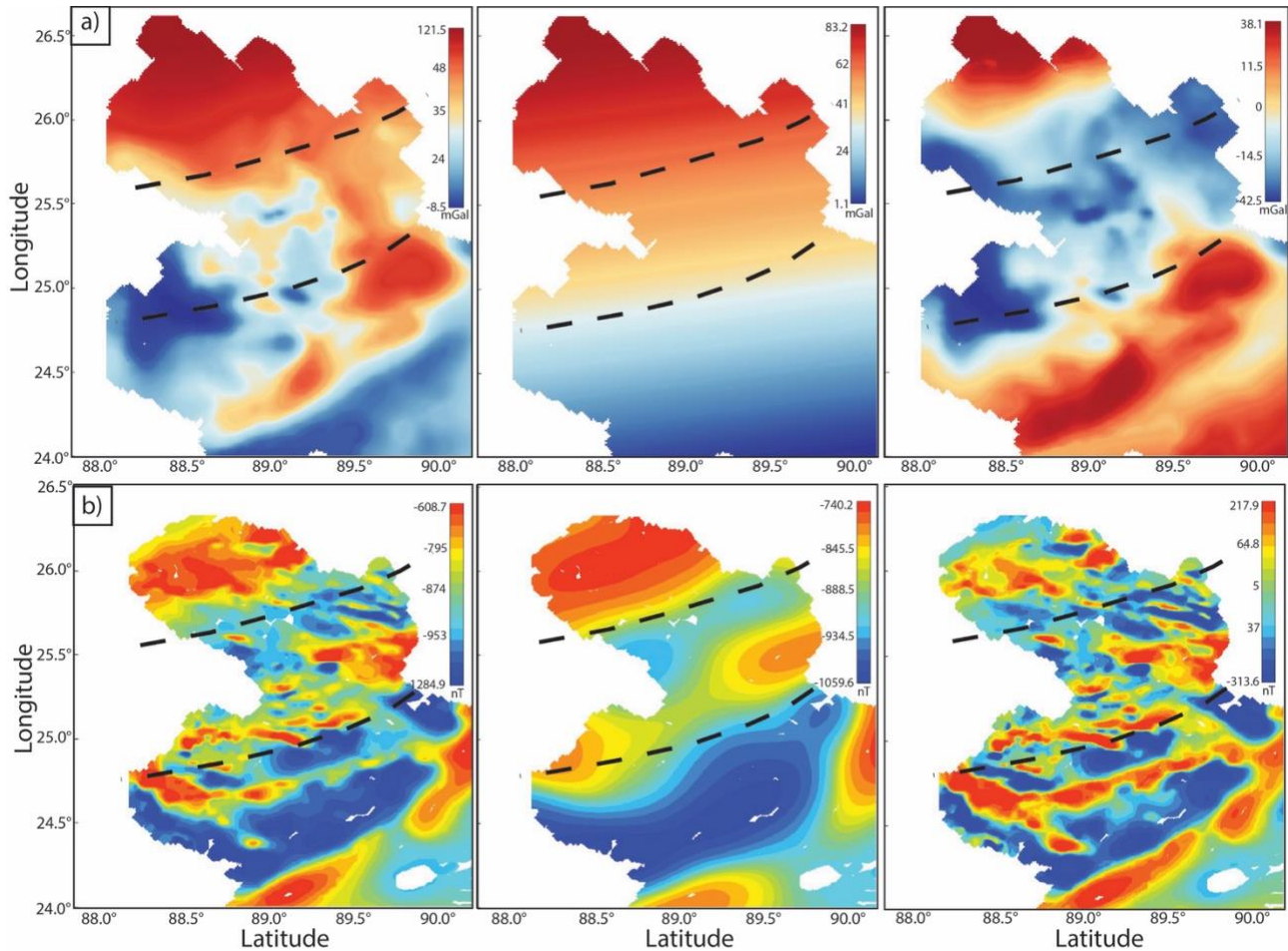
251 produce a stronger (high-amplitude) anomaly; if they are opposed or significantly misaligned, they
252 partially cancel or reorient the net magnetization, which can weaken the anomaly or even yield
253 one of opposite polarity compared to what an induced-only model would predict. This interplay
254 complicates data interpretation, since assuming all magnetization is induced (parallel to today's
255 field) can lead to errors in locating or characterizing sources.

256
257 By removing these regional trends, we enhance the visibility of smaller-scale or high-frequency
258 anomalies, allowing subtle features and variations in the subsurface to be highlighted more
259 effectively. To remove regional anomalies, we apply an upward continuation of 1000 m to the
260 Bouguer gravity data (**Figure 3a**). This approach simulates measuring the gravity field at a higher
261 elevation—1000 m in our case—effectively smoothing out high-frequency anomalies associated
262 with shallow or near-surface geological features (Balogun et al., 2023). For RTP magnetic
263 anomaly, we use a Gaussian filter to calculate the regional trend (**Figure 3b**). This Gaussian filter
264 acts as a low-pass filter, smoothing out high-frequency components in the dataset. After extracting
265 the regional anomaly from the potential field, we subtract it from the unfiltered total anomaly,
266 yielding the residual anomaly (**Figure 3**).

267
268 We apply several filters to the residual potential field data to enhance specific features and improve
269 interpretability (**Figure 3**). Under the framework of Poisson's theorem in potential-field theory,
270 taking a vertical derivative of gravity and performing a reduction-to-the-pole on magnetic data are
271 mathematically analogous operations and are equivalent Fourier-domain operations: both sharpen
272 source-edge contrasts while suppressing deep, long-wavelength signals, thus yielding mutually
273 consistent structural imagery (Blakely, 1996). The filters we have used involve various forms of
274 derivative operations, which help to highlight changes in the data that correspond to geological
275 boundaries, faults, or other structural details (Ibraheem et al., 2023; Ma et al., 2016; Nasuti et al.,
276 2019; Núñez-Demarco et al., 2023). For the residual RTP magnetic data, we apply and show two
277 filters: the horizontal derivative and the tilt derivative. The horizontal derivative filter, applied in
278 x-direction (i.e., across the longitudes) and y-direction (i.e., across the latitudes), accentuates
279 lateral changes in the magnetic field, helping to reveal abrupt variations. The tilt derivative filter,
280 however, is especially effective as an edge detector. It operates by combining both vertical and
281 horizontal gradients, effectively highlighting the edges of anomalous bodies. The tilt derivative
282 produces values that tend toward zero over magnetically flat regions, positive over rising areas,
283 and negative over falling areas, creating a clear demarcation of the edges of magnetic sources. As
284 a result, this filter enhances the boundaries of anomalies and helps pinpoint the locations and
285 shapes of features with minimal distortion across varying depths (Ashraf and Filina, 2023b; Pham
286 and Oliveira, 2023). We apply the lineament mapping techniques to map major structural
287 boundaries from the filtered magnetic data (Ashraf and Filina, 2023a, 2023b; Ogah and Abubakar,
288 2024; Zhang et al., 2024). Our approach focused on identifying gaps between magnetic stripes,
289 changes in the stripe orientation, and a significant reduction in stripe width. We also calculate the
290 analytical signals of the magnetic anomalies to highlight the areas with high magnetizing
291 amplitude (Nabighian, 1972; Roest and Pilkington, 1993) that may illuminate magnetic mineral
292 deposits (Mohamed et al., 2022). To calculate the analytical signal of the residual magnetic data,
293 we first compute the horizontal and vertical derivatives of the magnetic field in the x, y, and z
294 directions. The analytical signal was then derived by taking the square root of the sum of the
295 squares of these derivatives, yielding a map that represents the amplitude of the magnetic field
296 independent of direction and highlights the edges of magnetic sources. To validate our

297 interpretations, we cross-reference the magnetic lineaments with gravity data. Before validating
298 with gravity data, we filter the residual gravity data by applying the first vertical derivative and tilt
299 derivative to map major tectonic structures and delineate their boundaries.
300

301 We also develop 2-D integrated models of the subsurface to examine the variations in the physical
302 properties of the rocks (density and magnetic susceptibility). We build our models using the GM-
303 SYS module within the Geosoft software suite, employing a 2-D approximation (Geosoft, 2021).
304 The GM-SYS model is extended to +/- 30000 km (i.e., infinity) along the X-axis and 90 km along
305 the Z-axis to eliminate edge effects. Due to the absence of reliable magnetic susceptibility logs for
306 the sedimentary cover and granitic basement, we treat these lithologies as a non-magnetic
307 background (0 SI). This approximation reduces the non-uniqueness of the potential field problem,
308 ensuring that the modeled response is driven primarily by the lateral susceptibility contrast of the
309 target magnetic unit. By integrating gravity and magnetic data within this 2D context, we can
310 delineate major geological boundaries and assess regional structural trends with sufficient
311 accuracy for our research objectives. Our goal is to develop a simple subsurface structure that
312 satisfactorily aligns with gravity, magnetic, and logging data without introducing excessive
313 complexity that might overfit the potential field anomaly. Instead, we aim to replicate the general
314 pattern of the observed anomaly in our 2D modeling, seeking to generate computed anomalies
315 with comparable amplitude, wavelength, and phase to those observed in the potential fields.
316



317
318

319 Figure 3: Potential field data maps of northwestern Bangladesh used in this study to analyze geological and tectonic
320 features. (a) Gravity anomaly maps: from left to right, the Bouguer gravity anomaly, regional Bouguer gravity anomaly
321 with 1000 m upward continuation, and residual Bouguer gravity anomaly. (b) Magnetic anomaly maps: from left to
322 right, the RTP total magnetic anomaly, regional magnetic anomaly after Gaussian filtering, and residual magnetic
323 anomaly. The black dashed lines show the boundary of Rangpur Saddle.

324

325 **4. Result**

326

327 **4.1 Integrated spatial analysis**

328

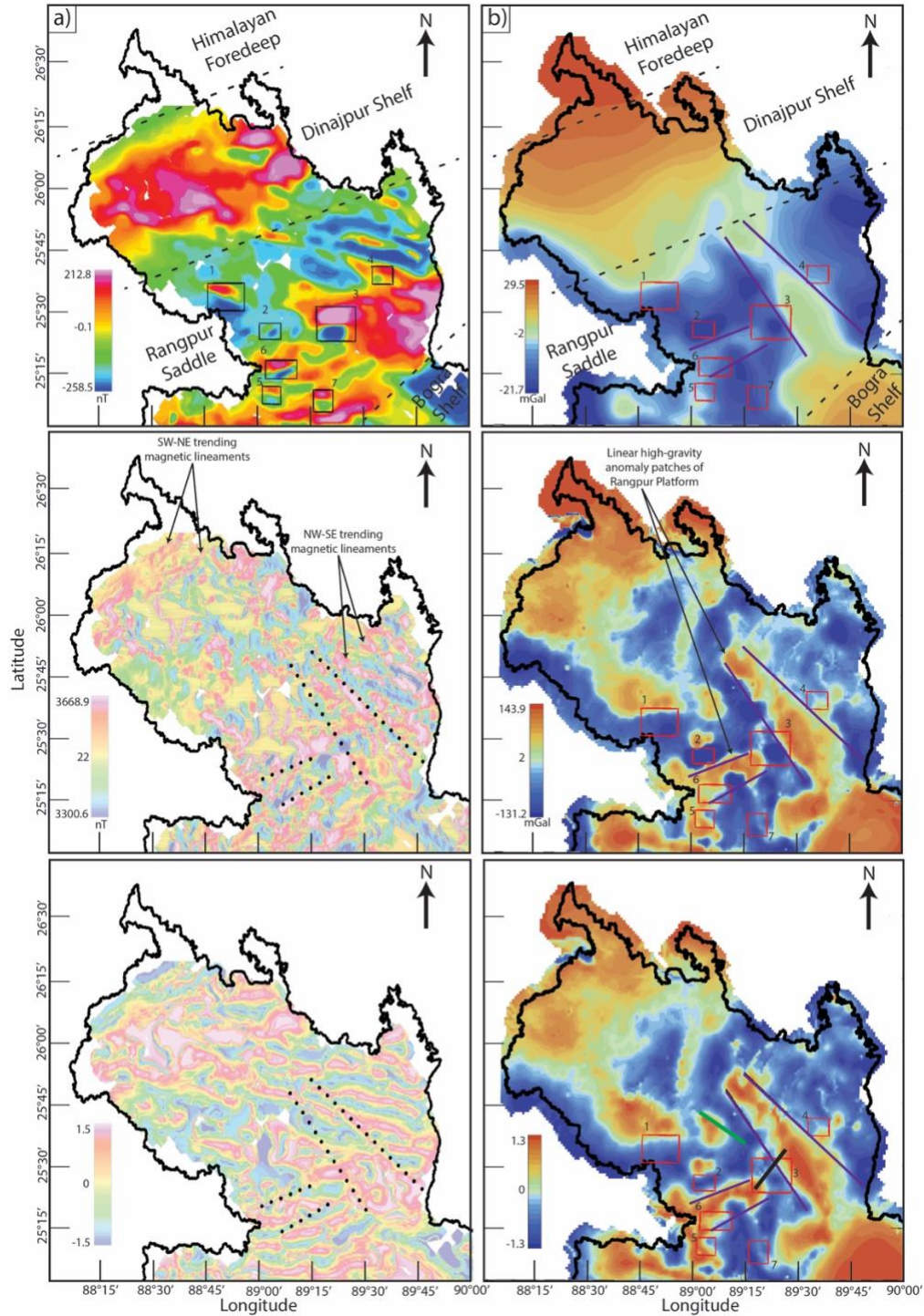
329 In this study, we first establish the regional tectonic structures of northwestern Bangladesh through
330 spatial analysis of multiple geophysical datasets. We utilize gravity, magnetic, seismic image
331 interpretations, and drilling log data to characterize the tectonic setup of this region. Our analysis
332 of residual magnetic and gravity anomalies reveals that the Rangpur Saddle exhibits distinctly
333 different geophysical characteristics compared to its northern counterpart, the Himalayan Foredeep
334 region. These differences are discernible in the long-wavelength or broad-scale geophysical
335 signatures across the two regions.

336

337 In the Himalayan Foredeep, north of 26°N latitude, we observe a high residual Bouguer gravity
338 anomaly, ranging from approximately 5 to 30 mGal. In contrast, the Rangpur Saddle, located south
339 of this latitude, is marked by a low residual Bouguer gravity anomaly, typically between -22 and
340 0 mGal. Similarly, the Rangpur Saddle shows lower residual RTP total magnetic anomalies,
341 ranging from 0 to 260 nT compared to mostly high magnetic anomalies in north (~ 0 to 215 nT).
342 The spatial patterns of these anomalies also differ across the regions. South of 26°N latitude, in
343 the Rangpur Saddle, the horizontal and tilt derivative magnetic anomalies show a predominance
344 of NW-SE trending magnetic lineaments. North of this latitude, in the Himalayan Foredeep, the
345 magnetic anomaly trend shifts predominantly to a SW-NE orientation. Additionally, in the vertical
346 and tilt derivatives of the gravity data, we observe the most pronounced high gravity linear
347 anomaly patch trends NW-SE south of 26°N latitude, consistent with the magnetic anomaly trend
348 in this area. South of 26°30'N latitude, we see another linear high-gravity patch in the filtered
349 Bouguer gravity data trending NW-SE, indicating a different orientation than the other high-
350 gravity patch of the Rangpur Saddle region. These two high-gravity patches are also traceable in
351 the filtered magnetic anomalies, following the magnetic lineament mapping procedure. Notably,
352 some areas exhibit strong inverse gravity and magnetic field trends, where high gravity coincides
353 with low magnetic anomalies, or vice versa. One might expect a corresponding increase in the
354 gravity signal due to the higher density of the gabbroic intrusions relative to the overlying rocks;
355 however, this expected gravity anomaly is not observed in our data. We believe this discrepancy
356 arises from two interconnected factors. First, gravity and magnetic methods are most sensitive to
357 lateral variations in subsurface properties, and in our study area, the subsurface structures are
358 predominantly flat-lying. At depth, the gabbroic intrusions are laterally adjacent to felsic basement
359 rocks, and while the density contrast between these lithologies is modest (~0.1 kg/m³), their
360 magnetic susceptibilities differ significantly. This contrast produces a strong magnetic response
361 but only a subtle gravity anomaly that may be indistinguishable from background variations. Also,
362 the intrusions occur in fault-bounded graben fill that causes a localized low density (due to thick
363 low-density Gondwana sediments in the graben). Second, the spatial resolution of our gravity
364 survey, with a station spacing of approximately 3 km, is relatively coarse compared to the scale of
365 the gabbroic intrusions. As a result, any high-frequency gravity signals associated with these

366 smaller or more localized bodies are likely undersampled and thus not adequately captured in the
367 final gravity dataset. In brief, the high gravity areas correspond to uplifted blocks of dense
368 basement, whereas the magnetic highs occur on the flanks where intrusions have come up along
369 faults and the graben is filled with lighter sediment, yielding a relative gravity low.

370
371 Within the Rangpur Saddle region, we observe multiple oval dipolar patterns. From the RTP
372 residual magnetic anomaly data, we identify seven distinct patterns. The identification of these
373 patterns follows several consistent criteria. First, the dipolar magnetic anomalies are generally
374 oriented in a north-south direction. Second, each pattern features a magnetic high in the northern
375 section and a corresponding low to the south. Third, within each pattern, the size, area, and
376 amplitude of the magnetic high and low anomalies are comparable, contributing to a symmetrical
377 structure. The filtered magnetic data also reveals possible signatures of remanently magnetized
378 sources, some of which may be reversely magnetized. At the Earth's magnetic field inclination of
379 approximately 45° in northwestern Bangladesh (based on the IGRF 1980 epoch used for RTP
380 correction), reversely magnetized sources such as gabbroic intrusions formed during past
381 geomagnetic reversals produce negative anomalies after RTP where positive anomalies would
382 align with the current field. Mapping these magnetic patterns onto the filtered gravity maps reveals
383 that they consistently lie near the boundary between high and low gravity anomalies. While most
384 of these magnetic patterns (patterns 1, 4, 5, 6, and 7) intersect only one boundary, a few patterns
385 (specifically patterns 2 and 3) touch boundaries on both sides.
386



387
 388 Figure 4: a) Magnetic anomaly maps of northwestern Bangladesh. The top panel displays the residual RTP total
 389 magnetic anomaly, the middle panel shows the first horizontal derivative in the x-direction (across longitudes), and
 390 the bottom panel illustrates the tilt derivative. Black boxes highlight areas where oval dipolar magnetic patterns are
 391 observed. Dotted black lines in the middle and bottom panels indicate boundaries of high gravity regions. b) Bouguer
 392 gravity anomaly maps of northwestern Bangladesh. The top panel presents the residual Bouguer gravity anomaly, the
 393 middle panel shows the first vertical derivative, and the bottom panel displays the tilt derivative. High gravity regions
 394 are outlined by purple solid lines, and red boxes indicate areas with dipolar magnetic patterns. The solid green line in
 395 the bottom panel represents seismic profile 2 from Figure 2. The thick solid black line shows the 2-D integrated
 396 modelling profile of Figure 5.

4.2 Integrated subsurface modeling

We develop a 2-D subsurface model utilizing gravity, magnetic, and drilling log data (**Figure 5**). The goal of this model is to approximate the observed anomalies on a local scale while aligning with the available drilling log information (**Figure 2c**). The magnetic anomaly modeled in **Figure 5** is the residual RTP anomaly, reflecting local high-frequency features after removing regional trends. Importantly, we do not aim to achieve a precise fit between the observed data and calculated anomalies. This decision is driven by the fact that the observed potential field data are influenced by regional structures, and without sufficient seismic information, constructing a reliable regional model is not feasible. Instead, we focus on developing a simplified version of the subsurface model that reasonably fits the observed anomalies and drilling data.

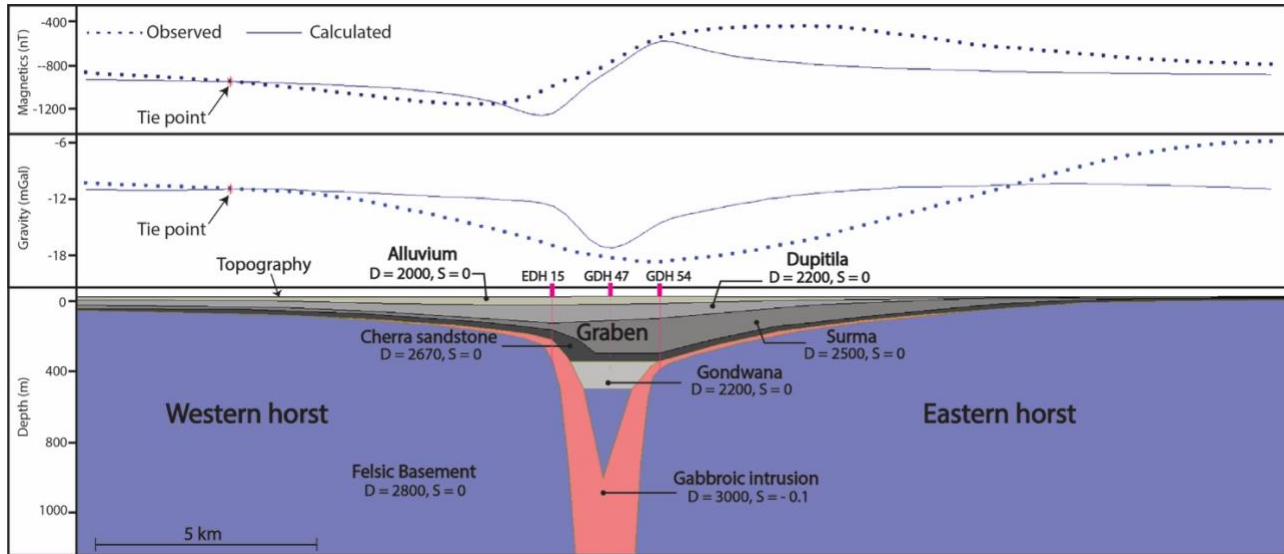
To ground the 2-D model in reality, we incorporated available drilling log information (**Figure 2**). Based on these logs, the model includes five sedimentary layers above a crystalline basement. The shallowest layer is assigned as alluvium, extending to a depth of 50 meters or less. Beneath the alluvium, we sequentially include the Dupitila, Surma, and Cherra sandstone layers. The variable thickness of these sedimentary layers comes from the drilling log information, except for the Gondwana layer. The thickness of Gondwana is approximated based on the gravity fit. Below these layers, we model a mafic intrusion of gabbro, which occurs within fault structures that have developed within the underlying felsic basement.

The resulting model indicates that a horst and graben structure is the most plausible configuration when considering the regional geological context. This structural interpretation also provides a reasonable match to the observed geophysical anomalies. Additionally, based on information from drilling log GDH 47, we assign a layer of Gondwana sediments within the graben basin, which is contributing to the low observed gravity in this region.

Densities in the model are derived from drilling data, reflecting the unique lithological characteristics of each unit. To get an initial guess on the density, we developed a gravity model for profile 1 that has seismic-derived subsurface information (**Figure S2**). The alluvium, Dupitila, Surma, and Cherra Sandstone layers are modeled with densities of 2000, 2200, 2500, and 2670 kg/m³, capturing their progressive compaction and mineral composition. The Gondwana unit, enriched with coal deposits, exhibits a notably lower density of 2200 kg/m³, consistent with its organic-rich composition. Beneath these layers, the felsic basement and gabbroic intrusion stand out with densities of 2800 and 3000 kg/m³, highlighting their denser crystalline structure and mafic origins.

Between 400 and 800 meters depth, the gabbroic intrusion begins to follow the fault plane. The thickness of both the Gondwana layer and the underlying felsic basement is determined from the amplitude of the calculated gravity and magnetic anomalies. The thickness of the Gondwana layer influences the minimum value of the calculated gravity anomaly, while the amplitude of the magnetic anomaly helps determine the depth of the gabbroic intrusion. Notably, our calculated anomalies are of high frequency. This occurs because our modeling does not incorporate all regional structures; instead, it focuses only on local structures. As a result, the calculated anomalies reflect primarily local or high-frequency potential field anomalies.

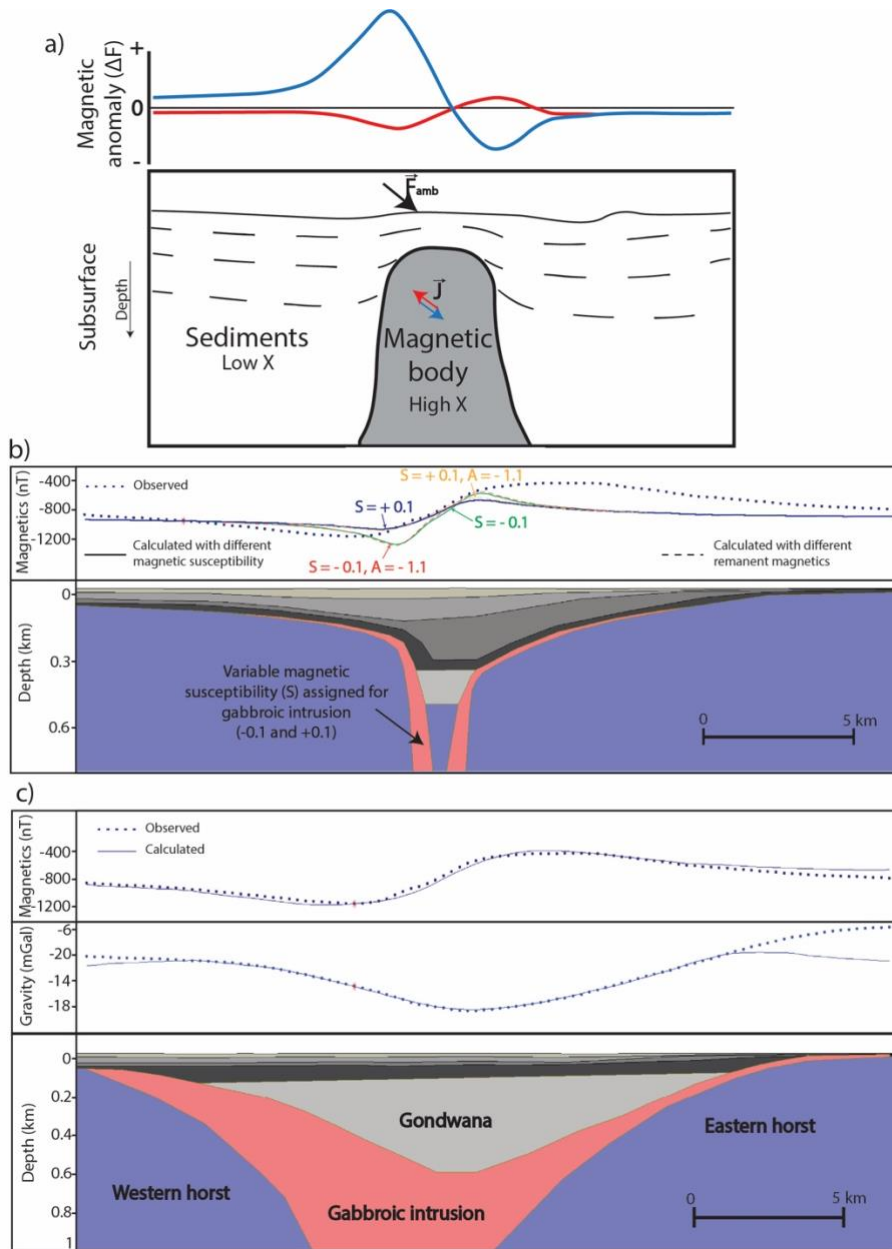
443 Our 2D subsurface model reveals two horst structures with a graben basin in the middle. We refer
 444 to these as the eastern and western horsts based on their geographic locations. In the model, the
 445 western horst structure is depicted as deeper, consistent with the observed gravity anomaly, which
 446 shows lower gravity in the western horst compared to the eastern horst. Our model does not include
 447 the broader horst structure on the eastern side, which likely explains the discrepancy between the
 448 calculated and observed anomalies over the eastern horst.
 449



450
 451
 452 Figure 5: Integrated 2D geophysical model over the highest magnetic anomaly in northwestern Bangladesh. See Figure
 453 1b and 4c for the location of the model profile. The top panel presents the total magnetic intensity anomaly, and the
 454 middle panel shows the gravity anomaly, with observed (dotted) and calculated (solid) data. Tie points, marked by red
 455 stars, indicate where the calculated anomalies are vertically shifted to align with the observed data. The bottom panel
 456 illustrates the subsurface model, with geological units represented by distinct colors. 'D' denotes density (kg/m^3), and
 457 'S' denotes magnetic susceptibility (SI units). Bold pink vertical dashes mark the locations of drilling logs used to
 458 constrain subsurface units. Thin vertical pink lines extend downward from these surface locations. Solid pink lines
 459 beneath EDH 15 and GDH 54 indicate where the forward model is directly tied to lithological boundaries from well
 460 logs. In contrast, the dashed pink line beneath GDH 47 reflects an interpretative connection, as this well does not lie
 461 directly along the modeling profile.

462
 463 We acknowledge the mismatch between the observed and calculated anomalies in our forward
 464 model. We aim to adopt the simplest model that captures the essential features of the observed
 465 anomaly without introducing unnecessary complexity. While even basic 2-D models can yield
 466 multiple valid solutions, incorporating intricate structures without strong geological constraints
 467 would increase interpretive ambiguity. Additionally, our model is inherently two-dimensional and
 468 thus cannot fully represent the three-dimensional geological variations present in the study area,
 469 such as the broad, shallow eastern horst, whose lateral extent likely contributes to higher observed
 470 gravity values. Finally, our modeling profile spans a smaller area than the full potential field survey
 471 (refer to section 3.1), resulting in calculated anomalies that emphasize localized, high-frequency
 472 features, whereas the observed data reflect broader, lower-frequency trends. Our forward model is
 473 calculated on 250 m spacing, whereas the gravity data were acquired every 1–1.5 km and the
 474 magnetic data every 5 km.
 475

476 Furthermore, we also test alternative models, which further support that the presented version
477 offers the most concise and geologically reasonable solution. First, we test how the polarization
478 direction of the remanent magnetization affects the total magnetic intensity reading of a dome-
479 shaped magnetic body (**Figure 6a**). We incorporate both remanent magnetization (A) and
480 magnetic susceptibility (S) in the forward model, which affects the total magnetic intensity and its
481 polarity (**Figure 6b**). When we assign only a positive susceptibility contrast ($S = +0.1$ SI) without
482 remanence, the calculated anomaly captures the general shape of the observed data more
483 accurately in terms of slope, but the amplitude (highs and lows) is notably lower than the observed
484 values. In contrast, using a reverse-polarity remanent magnetization yields calculated amplitudes
485 that closely match the observed highs and lows; however, the overall shape shows a poorer fit,
486 with significant mismatches in the slopes. Because of the better match for the amplitudes, we prefer
487 the reverse polarity for the magnetic body in our forward model. We also implemented an
488 additional component of remanent magnetization (A) to the magnetic body, fixed at -1.1 A/m, and
489 tested combinations such as $S = -0.1$ SI with $A = -0.1$ A/m and $S = +0.1$ SI with $A = -1.1$ A/m.
490 These combinations yielded a similar response, primarily increasing the amplitude of the anomaly
491 without changing the overall trend. In conclusion, while the additional remanent magnetization
492 component amplifies the anomaly magnitude, it does not significantly affect the trend or alter the
493 interpretation of the model. We have also developed a model that shows a perfect fit between the
494 observed and calculated anomaly (**Figure 6c**). However, to achieve that, we need to completely
495 abandon the constraints from well-logs and regional structural context based on gravity and
496 magnetic data. For these reasons, we adopt a simplified, geologically grounded model that
497 balances interpretive clarity with structural realism.
498



499
500
501
502
503
504
505
506
507
508
509
510
511
512
513

Figure 6: a) Conceptual illustration showing polarization direction of the remanent magnetization affecting the total magnetic intensity reading of a dome-shaped magnetic body. The synthetic total-field anomaly (ΔF) profiles are calculated for a concealed high-susceptibility intrusion beneath low-susceptibility sediments. The blue curve represents the response when magnetization is purely induced parallel to the present-day ambient field F_{amb} , producing a simple positive-negative (dipolar) signature. The red curve shows how the anomaly shape and amplitude are modified when an oblique remanent magnetization component J is added to the induced vector. b) Investigation on how incorporating both remanent magnetization (A) and magnetic susceptibility (S) in the forward model affects the total magnetic intensity and its polarity. c) 2-D forward modelling along the same profile as Figure 5, where we have achieved a perfect fit between the calculated and observed anomalies except for the model edges.

514 **5. Discussion**

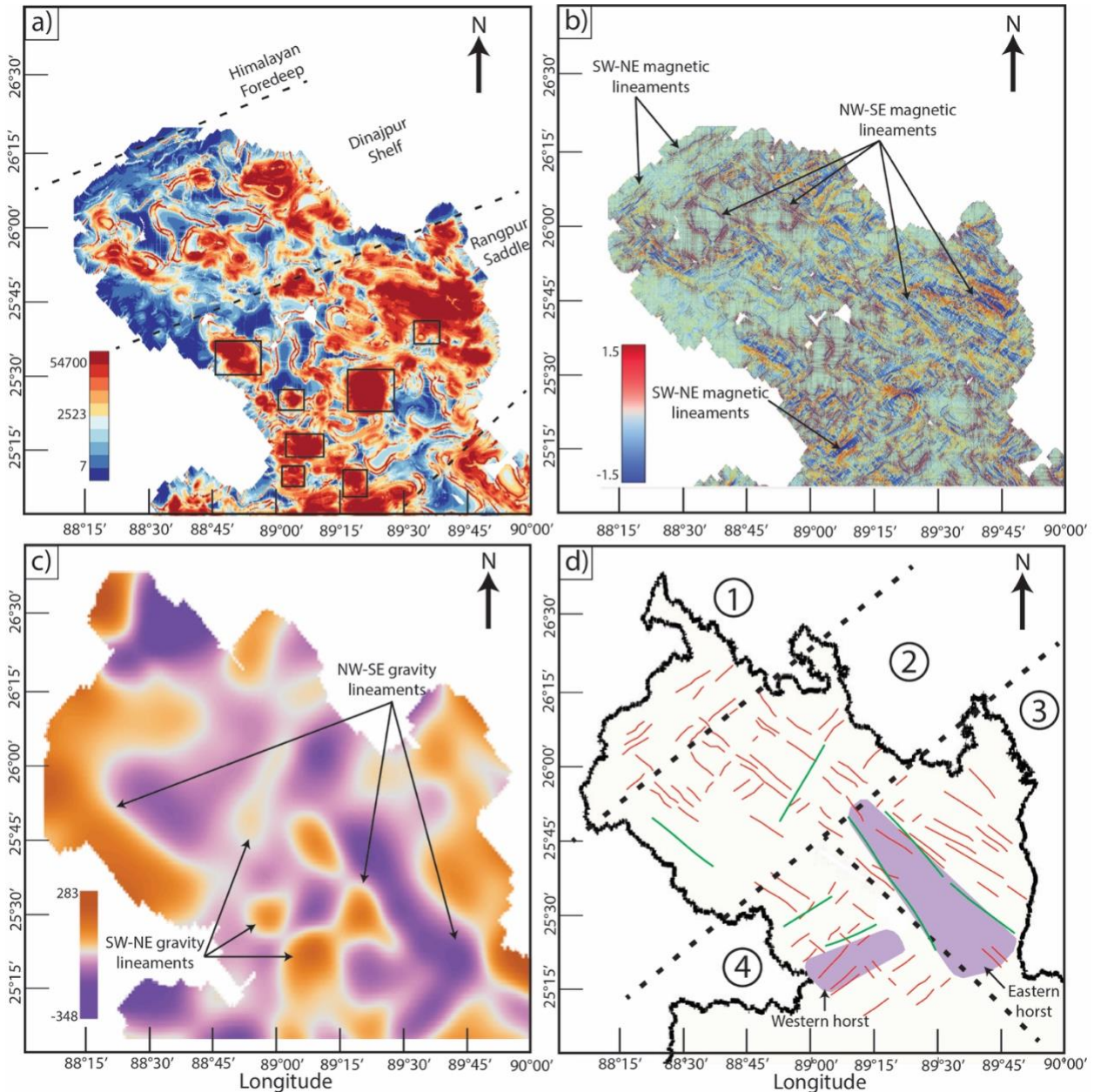
515 **5.1 Basement structure**

516
517
518 One of the primary goals of this paper is to understand the basement structure and tectonic setup
519 of the Rangpur Saddle. Our findings reveal significant differences in the basement structures of
520 the Rangpur Saddle compared to its northern counterparts, evident in both gravity and magnetic
521 data. A key distinction is the depth to basement between these regions (**Figure 1b**). Previous
522 studies consistently suggest that the basement depth in the Rangpur Saddle is shallower than in the
523 Dinajpur Shelf. However, those studies were based on limited seismic and drilling data. Our
524 results, however, indicate a more complex basement geometry than previously understood.
525 Filtered gravity and seismic data presented here suggest that the Rangpur Saddle region contains
526 both shallow and deep basement features (**Figure 4b**). Considering regional tectonics, we propose
527 that high gravity values correspond to shallow horst structures, while low gravity values indicate
528 deeper graben structures. However, the frequency of horsts and grabens is significantly lower in
529 the Rangpur Saddle compared to the northern Himalayan Foredeep and the Dinajpur Shelf (**Figure**
530 **2a** and **2b**). In the Rangpur region, we identified only two horsts of notable width and length. The
531 boundaries of these horst structures also appear as lineaments in the filtered magnetic data (**Figure**
532 **4a**), suggesting the presence of major structural boundaries.

533
534 Furthermore, differences in the directions of magnetic lineaments between the Rangpur Saddle
535 region and its northern counterparts—the Dinajpur Shelf and the Himalayan Foredeep—suggest
536 variations in paleo-tectonic stress orientation (**Figure 4a, 7a** and **7b**). Existing literature
537 characterizes northwestern Bangladesh predominantly with extensional tectonics (Gani and Alam,
538 2003). Near the Himalayan Foredeep boundary, SW-NE trending magnetic lineaments indicate a
539 paleo-principal stress direction oriented NW-SE. Moving southward into the Dinajpur Shelf, NW-
540 SE trending magnetic lineaments become more common (**Figure 7b**), pointing to a shift in the
541 principal stress direction associated with extensional tectonics. In the Rangpur Saddle, these NW-
542 SE trending lineaments are even more frequent, especially in the eastern part, indicating a greater
543 intensity of paleo-tectonic stress in this region compared to the Dinajpur Shelf. Based on traced
544 magnetic and gravity lineaments, the stable platform can be divided into four distinct zones
545 (**Figure 7d**). In Zone 1, located in the northern part, lineaments predominantly trend SW-NE, with
546 only a few exceptions. Moving southward into Zone 2, there is a mixture of two differently
547 trending lineaments: SW-NE and NW-SE. In Zone 3, in the easternmost section of the stable
548 platform, lineaments primarily trend NW-SE, aligning with the eastern horst. Finally, in Zone 4,
549 the southernmost region, lineaments generally follow an SW-NE trend, corresponding with the
550 western horst. This subdivision highlights the complex nature of past tectonic processes in this
551 region.

552
553 We also identify seven oval dipolar patterns of magnetic highs and lows. When mapped onto
554 gravity data, these patterns consistently align with the boundaries between high and low gravity
555 patches, indicating the possible boundaries between horsts and grabens. Drilling log data near the
556 most prominent magnetic anomaly reveals the presence of gabbro, which may explain these
557 dipolar magnetic patterns. Furthermore, these regions of dipolar magnetic patterns also spatially
558 correlate with overall high magnetization (**Figure 7a**). We propose that these gabbro formations

559 resulted from intrusions along normal faults, formed by extensional tectonics, which define the
 560 boundaries between horsts and grabens.
 561



562
 563 Figure 7: Filtered potential field maps of the northwestern stable platform region of Bangladesh, highlighting major
 564 tectonic structures and boundaries. (a) Analytical signal map derived from the magnetic anomaly (methodology
 565 detailed in Sect. 3), showing magnetization amplitudes across the region. Black boxes indicate areas of oval dipolar
 566 magnetic patterns, as shown in Figure 4a. Dashed lines represent boundaries between established tectonic
 567 subdivisions. (b) Total horizontal gradient map of the magnetic anomaly, calculated by applying a first horizontal
 568 derivative filter in the X-direction, followed by a first horizontal derivative filter in the Y-direction. (c) Total horizontal
 569 derivative (similar method as in 'b') of the residual gravity anomaly. This map is developed after applying upward
 570 continuation to the residual gravity data to a level where high-resolution artifacts are no longer present in the derivative
 571 map. (d) Map displaying traced magnetic lineaments (in red) from 'b' and gravity lineaments (in green) from 'c'.
 572 Black dashed lines indicate regional subdivisions based on mapped tectonic lineaments. Purple polygons mark horst
 573 structures in the Rangpur Saddle, interpreted from filtered gravity data (refer to Figure 4b).

574

575 **5.2 Economic mineral potential**

576

577 Our integrated spatial analysis and 2-D modeling reveal that the Rangpur Saddle contains at least
578 two prominent horst and graben structures. The 2-D model results (**Figure 5**), supported by drilling
579 log data, confirm the presence of gabbroic bodies along normal faults within these structures. This
580 suggests that the most prominent oval-shaped dipolar magnetic signature has strong potential to
581 host iron-bearing rocks such as gabbro. When the other similar patterns are mapped onto the
582 gravity data, they consistently correspond to the boundaries between high and low gravity zones,
583 marking the transitions between horsts and grabens. We interpret these gabbroic intrusions as
584 products of magmatic emplacement along extensional faults (**Figure 8**), consistent with processes
585 associated with the early stages of continental rifting. Furthermore, analysis of lineament
586 orientations (**Figure 7d**) indicates that, except in the western horst region, most of the interpreted
587 magmatic emplacement appears to be controlled by NW–SE oriented lineaments.

588

589 The breakup process involved rifting events that progressively separated the Indian subcontinent
590 from the other Gondwanaland constituents (Veevers, 2004). The breakup of Gondwanaland
591 involved multiple rifting episodes and magmatic activities. While the Central Atlantic Magmatic
592 Province (CAMP) exemplifies rift-related magmatism during the Triassic-Jurassic breakup of
593 Pangea, the Rangpur Saddle's tectonic evolution is more directly tied to the Cretaceous rifting of
594 the Indian plate from Antarctica-Australia (Curry, 1991; Hossain et al., 2019). This rifting
595 facilitated extensional faulting and mafic intrusions, analogous to processes observed in CAMP
596 but occurring later in the Mesozoic. In such tectonic settings, normal faulting and rift-related
597 subsidence create pathways for mafic magmas to ascend (Brune et al., 2023; Pirajno and Santosh,
598 2014; Ruppel, 1995), leading to the emplacement of gabbroic and other mafic intrusions within
599 the crust (Magee et al., 2019).

600

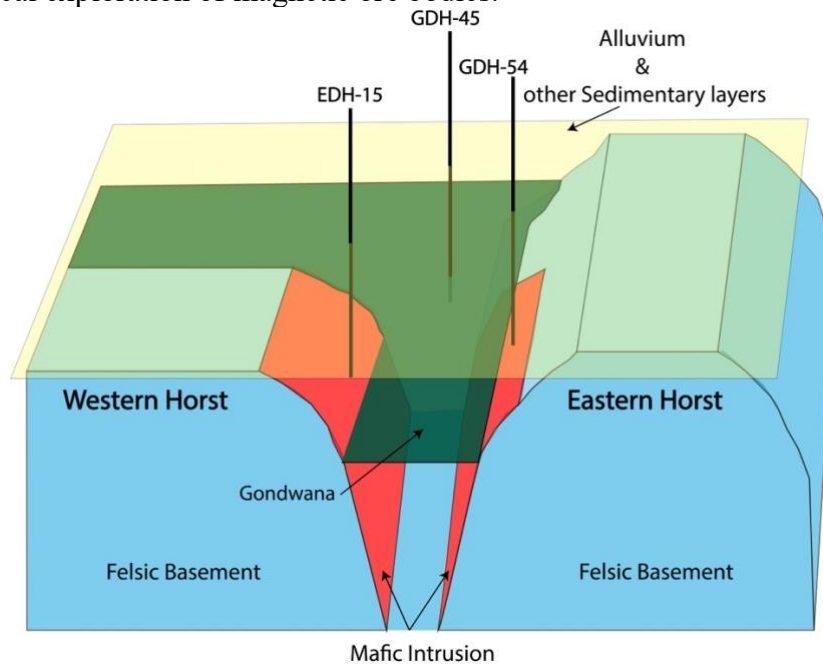
601 Mafic magma intrusions are commonly observed along extensional fault planes in tectonically
602 active regions worldwide. Troll et al. (2021) shows that in NW Scotland, Long Loch Fault acted
603 as dynamic magma conduit with its movements facilitating the ascent of ultrabasic magmas. These
604 magmas intruded along faults and fractures, leading to the destabilization and collapse of existing
605 cumulate layers, forming extensive breccias. A study on Mesozoic gabbroic intrusions in the High
606 Atlas Mountains highlights their emplacement along extensional faults during the rifting
607 associated with the Central Atlantic Magmatic Province, where more than 50% of gabbro samples
608 exhibit stable magnetization from magnetite which is identified as the primary component (Calvín
609 et al., 2017). Fuller and Waters (1929) have extensively studied horsts and graben structures in
610 southern Oregon where they found emplacement of volcanic and intrusive rocks are closely
611 associated with extensional faulting. These normal faults and the resulting grabens provide
612 pathways for magma to ascend and intrude, which is evident from the prevalence of rhyolitic,
613 dacitic, and andesitic vents as well as basaltic dikes aligned with the faults.

614

615 Mafic intrusions along fault zones are often associated with magnetic mineral deposits, which can
616 be economically significant as ore bodies (Zhou et al., 2005). For instance, magnetite deposits are
617 found within mafic intrusions along the fault planes in Egypt, which exhibit high magnetic
618 anomalies, facilitating their detection and delineation (Kharbish et al., 2022; Mousa et al., 2020).

619 Also, in Central Iran, iron-bearing magnetic mineral deposits are observed to exhibit high magnetic
620 and gravity anomalies (Kheyrollahi et al., 2021).

621
622 Based on current geochemistry data, the Rangpur Saddle holds significant potential for magnetic
623 mineral ore deposits, driven by its mafic-ultramafic sequences and iron-rich dykes (Ameen et al.,
624 2021). High Fe_2O_3 content in hornblendites and associated minerals like magnetite and ilmenite
625 indicate strong magnetization. The tectonic setting, with extensive magmatic intrusions, provides
626 ideal conditions for mineralization. These findings highlight the region as a possible target for
627 future geophysical exploration of magnetic ore bodies.



628
629
630 Figure 8: 3D schematic diagram illustrating the tectonic structures in Pirganj, where the highest magnetic anomaly is
631 observed in Bangladesh. The felsic basement, depicted in blue blocks, includes two horsts, as shown in Figure 5d.
632 Possible mafic intrusions along the faults are indicated in red. Sedimentary layers are represented by a single horizontal
633 layer in specific colors, with the graben basin likely filled with Gondwana sediments shown in green, and other
634 sedimentary layers, including alluvium, shown in yellow, which also represents the topography of the region. The
635 approximate locations of the three drilling logs used in this study (refer to Figure 1b for their locations) are also
636 indicated.

637 638 **5.3 Limitations and Future Research**

639
640 Compared to other regions globally, limited published research exists for our study area, restricting
641 our ability to draw on established models and findings. Situated at the eastern edge of the Indian
642 Shield, this area transitions into a different tectonic subdivision, creating a tectonic complexity
643 that cannot be fully resolved with the available low-resolution data. The scarcity of high-resolution
644 datasets, such as regional-scale seismic surveys, further limits our capacity to delineate regional
645 structures accurately. Currently, no regional or localized high-resolution datasets from ground-
646 based surveys are widely available, though such data could enhance future studies. Additionally,
647 the available well log data are predominantly shallow, reaching depths of approximately 500
648 meters, which limits insights into deeper geological and tectonic features beyond 2 kilometers.
649 Petrographic descriptions of the basement rocks are also rudimentary, as they are primarily based

650 on a limited number of well logs, most of which were drilled before the 1990s, leaving significant
651 gaps in our understanding of the area's deeper subsurface geology.

652
653 Future research in this region will focus on constructing detailed three-dimensional (3D) models
654 of the subsurface to enhance our understanding of the geological framework. This will involve
655 compiling a comprehensive dataset repository that integrates historical seismic reflection data,
656 including those acquired by private entities. Given the shallow nature of the basement, which lies
657 between approximately 128 and 1000 meters depth, high-resolution gravity and magnetic data will
658 be critical for resolving fine-scale structural features. To achieve the necessary spatial resolution,
659 precision ground-based gravity and magnetic surveys are recommended. Specifically, we propose
660 a targeted geophysical survey in areas exhibiting oval-shaped dipolar magnetic anomalies, using
661 station spacing of 500 meters or less. Such high-density measurements will improve our ability to
662 detect and delineate narrow mafic intrusions at shallow depths. In addition, developing a regional
663 tomographic model using either local earthquake data or ambient seismic noise will provide
664 complementary constraints on subsurface structures and further refine interpretations of the
665 geological setting.

666
667 The study area is characterized by complex tectonic structures shaped by a diverse tectonic history.
668 While the current study has focused on the Rangpur Saddle, future research will expand to cover
669 the entire northwestern part of Bangladesh, including the Himalayan Foredeep and the Eocene
670 Hinge region, which represents a Paleocontinental shelf. Such expanded coverage will provide
671 deeper insights into the tectonic evolution and geological complexity of the area.

672

673 **Conclusion**

674

675 This study provides a geophysical investigation of the northwestern region of Bangladesh,
676 revealing its significant potential for mineral resource exploration. The integration of gravity,
677 magnetic, seismic, and drilling data has allowed us to identify key tectonic features, such as
678 gabbroic intrusions along extensional faults, some which may host of valuable magnetic mineral
679 deposits. Despite the limitations in data resolution and coverage, our findings offer important
680 insights into the region's geological evolution and resource potential. Future work should prioritize
681 acquiring more detailed geophysical data and expanding drilling campaigns to refine the
682 understanding of subsurface structures and evaluate the feasibility of mineral extraction. The
683 Rangpur Saddle, as the shallowest part of the stable platform, emerges as a promising target for
684 future mineral exploration endeavors.

685

686 **Data availability**

687

688 All raw data can be provided by the corresponding authors upon request.

689

690 **Author contribution**

691

692 Mohammad Tawhidur Rahman Tushar was involved in conceptualization, methodology, software,
693 validation, formal analysis, investigation, resources, data curation, writing – original draft, writing
694 – review and editing, visualization. Asif Ashraf contributed to conceptualization, methodology,

695 software, validation, formal analysis, investigation, resources, data curation, writing – original
696 draft, writing – review and editing, and visualization. Md. Mahfuz Alam worked on software
697 development, validation, and formal analysis. Md Nasif Jamil contributed to writing – review and
698 editing and visualization. Saba Karim was involved in writing – review and editing and
699 visualization. Md. Shahjahan contributed to conceptualization, investigation, resources, project
700 administration, and supervision. Md. Anwar Hossain Bhuiyan was involved in writing – review
701 and editing, project administration, supervision, and funding acquisition.

702

703 **Competing interests**

704

705 The authors declare that they have no conflict of interest.

706

707 **Acknowledgment**

708

709 The gravity, magnetic, and seismic data, along with drilling information used in this study, were
710 graciously provided by the Geological Survey of Bangladesh (GSB), and the authors deeply
711 appreciate their support and collaboration. The authors also thank Asef Jamil Ajwad for his
712 assistance with computational facilities during the research. Special acknowledgment is made for
713 the Oasis Montaj classroom subscription and for the use of Geosoft Oasis Montaj v8.4 for data
714 processing and modeling. Finally, gratitude is extended to the Department of Geology, University
715 of Dhaka, for providing access to essential infrastructure and resources.

716

717 **Financial support**

718

719 This work was funded by the National Science and Technology Fellowship, awarded by the
720 Ministry of Science and Technology, Bangladesh.

721

722 **References**

723

724 Adebiyi, L. S., Eluwole, A. B., Fajana, A. O., Salawu, N. B., and Saleh, A.: Contrasting structures
725 of the Southern Benue trough and the contiguous crystalline basement as observed from high-
726 resolution aeromagnetic data, *Sci Rep*, 13, 21516, <https://doi.org/10.1038/s41598-023-48639-8>,
727 2023.

728 Ahamed, S., Hossain, D., and Alam, J.: Exploring Basement Surface relationship of north-west
729 Bengal Basin using satellite images and tectonic modeling,
730 <https://doi.org/10.48550/ARXIV.2004.02734>, 2020.

731 Akhtar, A.: Mineral resources and their economic significance in national development:
732 Bangladesh perspective, *SP*, 250, 127–134, <https://doi.org/10.1144/GSL.SP.2005.250.01.12>,
733 2005.

734 Alam, M.: Geology and depositional history of Cenozoic sediments of the Bengal Basin of
735 Bangladesh, *Palaeogeography, Palaeoclimatology, Palaeoecology*, 69, 125–139,
736 [https://doi.org/10.1016/0031-0182\(89\)90159-4](https://doi.org/10.1016/0031-0182(89)90159-4), 1989.

- 737 Alam, M., Alam, M. M., Curray, J. R., Chowdhury, M. L. R., and Gani, M. R.: An overview of
738 the sedimentary geology of the Bengal Basin in relation to the regional tectonic framework and
739 basin-fill history, *Sedimentary Geology*, 155, 179–208, [https://doi.org/10.1016/S0037-](https://doi.org/10.1016/S0037-0738(02)00180-X)
740 [0738\(02\)00180-X](https://doi.org/10.1016/S0037-0738(02)00180-X), 2003.
- 741 Alken, P., Thébault, E., Beggan, C. D., Amit, H., Aubert, J., Baerenzung, J., Bondar, T. N., Brown,
742 W. J., Califf, S., Chambodut, A., Chulliat, A., Cox, G. A., Finlay, C. C., Fournier, A., Gillet, N.,
743 Grayver, A., Hammer, M. D., Holschneider, M., Huder, L., Hulot, G., Jager, T., Kloss, C., Korte,
744 M., Kuang, W., Kuvshinov, A., Langlais, B., Léger, J.-M., Lesur, V., Livermore, P. W., Lowes, F.
745 J., Macmillan, S., Magnes, W., Manda, M., Marsal, S., Matzka, J., Metman, M. C., Minami, T.,
746 Morschhauser, A., Mound, J. E., Nair, M., Nakano, S., Olsen, N., Pavón-Carrasco, F. J., Petrov,
747 V. G., Ropp, G., Rother, M., Sabaka, T. J., Sanchez, S., Saturnino, D., Schnepf, N. R., Shen, X.,
748 Stolle, C., Tangborn, A., Tøffner-Clausen, L., Toh, H., Torta, J. M., Varner, J., Vervelidou, F.,
749 Vigneron, P., Wardinski, I., Wicht, J., Woods, A., Yang, Y., Zeren, Z., and Zhou, B.: International
750 Geomagnetic Reference Field: the thirteenth generation, *Earth Planets Space*, 73, 49,
751 <https://doi.org/10.1186/s40623-020-01288-x>, 2021.
- 752 Ameen, S. M. M., Wilde, S. A., Kabir, Md. Z., Akon, E., Chowdhury, K. R., and Khan, Md. S. H.:
753 Paleoproterozoic granitoids in the basement of Bangladesh: A piece of the Indian shield or an
754 exotic fragment of the Gondwana jigsaw?, *Gondwana Research*, 12, 380–387,
755 <https://doi.org/10.1016/j.gr.2007.02.001>, 2007.
- 756 Ameen, S. M. M., Tapu, A.-T., and Hossain, M. S.: Precambrian Basement Rock of Bangladesh
757 and Its Metallic Minerals, in: *Bangladesh geosciences and resources potential*, CRC Press Books,
758 25–54, 2021.
- 759 Arkani-Hamed, J.: Differential reduction to the pole: Revisited, *GEOPHYSICS*, 72, L13–L20,
760 <https://doi.org/10.1190/1.2399370>, 2007.
- 761 Ashraf, A. and Filina, I.: New 2.75-D gravity modeling reveals the low-density nature of
762 propagator wakes in the Juan de Fuca plate, *Tectonophysics*, 869, 230127,
763 <https://doi.org/10.1016/j.tecto.2023.230127>, 2023a.
- 764 Ashraf, A. and Filina, I.: Zones of Weakness Within the Juan de Fuca Plate Mapped From the
765 Integration of Multiple Geophysical Data and Their Relation to Observed Seismicity, *Geochem*
766 *Geophys Geosyst*, 24, e2023GC010943, <https://doi.org/10.1029/2023GC010943>, 2023b.
- 767 Balogun, O. B., Akereke, O. F., and Nwobodo, A. D.: Understanding the Constraints to the Correct
768 Application of the Upward Continuation Operation in Gravity Data Processing, *Pure Appl.*
769 *Geophys.*, 180, 3787–3811, <https://doi.org/10.1007/s00024-023-03348-1>, 2023.
- 770 Blakely, R. J.: *Potential theory in gravity and magnetic applications*, Cambridge university press,
771 1996.
- 772 Brune, S., Kolawole, F., Olive, J.-A., Stamps, D. S., Buck, W. R., Buitter, S. J. H., Furman, T., and
773 Shillington, D. J.: Geodynamics of continental rift initiation and evolution, *Nat Rev Earth Environ*,
774 4, 235–253, <https://doi.org/10.1038/s43017-023-00391-3>, 2023.

775 Calvin, P., Ruiz-Martínez, V. C., Villalaín, J. J., Casas-Sainz, A. M., and Moussaid, B.:
776 Emplacement and Deformation of Mesozoic Gabbros of the High Atlas (Morocco):
777 Paleomagnetism and Magnetic Fabrics, *Tectonics*, 36, 3012–3037,
778 <https://doi.org/10.1002/2017TC004578>, 2017.

779 Chowdhury, K. R., Hossain, M. S., and Khan, M. S. H. (Eds.): *Bangladesh geosciences and
780 resources potential*, First edition., CRC Press, Boca Raton, 610 pp., 2022.

781 Curray, J. R.: Geological history of the Bengal geosyncline, *Journal of Association of Exploration
782 Geophysicists*, 12, 209–219, 1991.

783 Curray, J. R. and Moore, D. G.: Sedimentary and Tectonic Processes in the Bengal Deep-Sea Fan
784 and Geosyncline, in: *The Geology of Continental Margins*, edited by: Burk, C. A. and Drake, C.
785 L., Springer Berlin Heidelberg, Berlin, Heidelberg, 617–627, [https://doi.org/10.1007/978-3-662-
786 01141-6_45](https://doi.org/10.1007/978-3-662-01141-6_45), 1974.

787 DeCelles, P. G.: Foreland Basin Systems Revisited: Variations in Response to Tectonic Settings,
788 in: *Tectonics of Sedimentary Basins*, edited by: Busby, C. and Azor, A., Wiley, 405–426,
789 <https://doi.org/10.1002/9781444347166.ch20>, 2011.

790 Filina, I., Biegert, E. K., Sander, L., Tschirhart, V., Bundalo, N., and Schiek-Stewart, C.: Integrated
791 imaging: A powerful but undervalued tool, *The Leading Edge*, 38, 720–724,
792 <https://doi.org/10.1190/tle38090720.1>, 2019.

793 Fuller, R. E. and Waters, A. C.: The Nature and Origin of the Horst and Graben Structure of
794 Southern Oregon, *The Journal of Geology*, 37, 204–238, 1929.

795 Hasan, M. M., Monir, A., and Hassan, M.: Evaluating the Energy and Mineral Resources Prospect
796 and Future Development in Bangladesh: A Review, <https://doi.org/10.2139/ssrn.4484598>, 2023.

797 Hendrickson, M. D.: Geologic interpretation of aeromagnetic and chemical data from the Oaks
798 Belt, Wabigoon subprovince, Minnesota: implications for Au-rich VMS deposit exploration, *Can.
799 J. Earth Sci.*, 53, 176–188, <https://doi.org/10.1139/cjes-2015-0141>, 2016.

800 Hildenbrand, T. G.: Regional Crustal Structures and Their Relationship to the Distribution of Ore
801 Deposits in the Western United States, Based on Magnetic and Gravity Data, *Economic Geology*,
802 95, 1583–1603, <https://doi.org/10.2113/95.8.1583>, 2000.

803 Hossain, I., Tsunogae, T., Rajesh, H. M., Chen, B., and Arakawa, Y.: Palaeoproterozoic U–Pb
804 SHRIMP zircon age from basement rocks in Bangladesh: A possible remnant of the Columbia
805 supercontinent, *Comptes Rendus Geoscience*, 339, 979–986,
806 <https://doi.org/10.1016/j.crte.2007.09.014>, 2007.

807 Hossain, Md. S., Khan, Md. S. H., Chowdhury, K. R., and Abdullah, R.: Synthesis of the Tectonic
808 and Structural Elements of the Bengal Basin and Its Surroundings, in: *Tectonics and Structural
809 Geology: Indian Context*, edited by: Mukherjee, S., Springer International Publishing, Cham, 135–
810 218, https://doi.org/10.1007/978-3-319-99341-6_6, 2019.

811 Ibraheem, I. M., Tezkan, B., Ghazala, H., and Othman, A. A.: A New Edge Enhancement Filter
812 for the Interpretation of Magnetic Field Data, *Pure Appl. Geophys.*, 180, 2223–2240,
813 <https://doi.org/10.1007/s00024-023-03249-3>, 2023.

814 Jaffal, M., Goumi, N. E., Kchikach, A., Aïfa, T., Khattach, D., and Manar, A.: Gravity and
815 magnetic investigations in the Haouz basin, Morocco. Interpretation and mining implications,
816 *Journal of African Earth Sciences*, 58, 331–340, <https://doi.org/10.1016/j.jafrearsci.2010.03.012>,
817 2010.

818 Jain, A. K., Banerjee, D. M., and Kale, V. S.: *Tectonics of the Indian Subcontinent*, Springer
819 International Publishing, Cham, <https://doi.org/10.1007/978-3-030-42845-7>, 2020.

820 Kabir, Z. M., Chowdhury, K. R., Akon, E., Kazi, A. I., and Ameen, S. M. M.: Petrogenetic Study
821 of Precambrian Basement Rocks from Maddhapara, Dinajpur, Bangladesh, *Bangladesh*
822 *Geoscience Journal*, 7, 1–18, 2001.

823 Khan, A. A. and Rahman, T.: An analysis of the gravity field and tectonic evaluation of the
824 northwestern part of Bangladesh, *Tectonophysics*, 206, 351–364, [https://doi.org/10.1016/0040-](https://doi.org/10.1016/0040-1951(92)90386-K)
825 [1951\(92\)90386-K](https://doi.org/10.1016/0040-1951(92)90386-K), 1992.

826 Khan, F. H.: *Geology of Bangladesh*, 1991.

827 Kharbish, S., Eldosouky, A. M., and Amer, O.: Integrating mineralogy, geochemistry and
828 aeromagnetic data for detecting Fe–Ti ore deposits bearing layered mafic intrusion, Akab El-
829 Negum, Eastern Desert, Egypt, *Sci Rep*, 12, 15474, <https://doi.org/10.1038/s41598-022-19760-x>,
830 2022.

831 Kheyrollahi, H., Alinia, F., and Ghods, A.: Regional magnetic and gravity structures and
832 distribution of mineral deposits in Central Iran: Implications for mineral exploration, *Journal of*
833 *Asian Earth Sciences*, 217, 104828, <https://doi.org/10.1016/j.jseaes.2021.104828>, 2021.

834 Ma, G., Huang, D., and Liu, C.: Step-Edge Detection Filters for the Interpretation of Potential
835 Field Data, *Pure Appl. Geophys.*, 173, 795–803, <https://doi.org/10.1007/s00024-015-1053-6>,
836 2016.

837 Magee, C., Ernst, R. E., Muirhead, J., Phillips, T., and Jackson, C. A.: Magma transport pathways
838 in large igneous provinces: lessons from combining field observations and seismic reflection data,
839 in: *Dyke Swarms of the World: A Modern Perspective*, 45–85, 2019.

840 Masum, M., Hoque, M. N., Akbar, M. A., Mahmud, Z., Rana, M. S., Razzaque, M. A., and Amin,
841 M. A.: Geology and Precambrian Banded Iron Formation formed at Rangpur Platform in
842 Bangladesh, *International Journal Of Engineering Research And Development*, 17, 43–57, 2021.

843 McCafferty, A. E., Stoesser, D. B., and Van Gosen, B. S.: Geophysical interpretation of U, Th, and
844 rare earth element mineralization of the Bokan Mountain peralkaline granite complex, Prince of
845 Wales Island, southeast Alaska, *Interpretation*, 2, SJ47–SJ63, [https://doi.org/10.1190/INT-2014-](https://doi.org/10.1190/INT-2014-0010.1)
846 [0010.1](https://doi.org/10.1190/INT-2014-0010.1), 2014.

- 847 Mohamed, A., Abdelrady, M., Alshehri, F., Mohammed, M. A., and Abdelrady, A.: Detection of
848 Mineralization Zones Using Aeromagnetic Data, *Applied Sciences*, 12, 9078,
849 <https://doi.org/10.3390/app12189078>, 2022.
- 850 Moon, J. W.: *The Mineral Industry of Bangladesh*, U.S. Geological Survey, 2022.
- 851 Morgan, J. P. and McIntire, W. G.: Quaternary Geology of The Bengal Basin, East Pakistan And
852 India, *Geol Soc America Bull*, 70, 319, [https://doi.org/10.1130/0016-7606\(1959\)70\[319:QGOTBB\]2.0.CO;2](https://doi.org/10.1130/0016-7606(1959)70[319:QGOTBB]2.0.CO;2), 1959.
- 854 Mousa, S. A. W., Abdel Nabi, S. H., Araffa, S. A. S., Mansour, S. A., and Al Deep, M. A. I.:
855 Geophysical exploration of titanomagnetite ore deposits by geomagnetic and geoelectric methods,
856 *SN Appl. Sci.*, 2, 444, <https://doi.org/10.1007/s42452-020-2206-5>, 2020.
- 857 Mukhopadhyay, D. and Matin, A.: Recent Studies on the Singhbhum Craton, *PINSA*, 86,
858 <https://doi.org/10.16943/ptinsa/2020/49788>, 2020.
- 859 Nabighian, M. N.: The Analytic Signal of Two-Dimensional Magnetic Bodies With Polygonal
860 Cross-Section: Its Properties And Use For Automated Anomaly Interpretation, *Geophysics*, 37,
861 507–517, <https://doi.org/10.1190/1.1440276>, 1972.
- 862 Nasuti, Y., Nasuti, A., and Moghadas, D.: STDR: A Novel Approach for Enhancing and Edge
863 Detection of Potential Field Data, *Pure Appl. Geophys.*, 176, 827–841,
864 <https://doi.org/10.1007/s00024-018-2016-5>, 2019.
- 865 Núñez-Demarco, P., Bonilla, A., Sánchez-Bettucci, L., and Prezzi, C.: Potential-Field Filters for
866 Gravity and Magnetic Interpretation: A Review, *Surv Geophys*, 44, 603–664,
867 <https://doi.org/10.1007/s10712-022-09752-x>, 2023.
- 868 Ogah, A. J. and Abubakar, F.: Solid mineral potential evaluation using integrated aeromagnetic
869 and aeroradiometric datasets, *Sci Rep*, 14, 1637, <https://doi.org/10.1038/s41598-024-52270-6>,
870 2024.
- 871 Pham, L. T. and Oliveira, S. P.: Edge Enhancement of Magnetic Sources Using the Tilt Angle and
872 Derivatives of Directional Analytic Signals, *Pure Appl. Geophys.*, 180, 4175–4189,
873 <https://doi.org/10.1007/s00024-023-03375-y>, 2023.
- 874 Pirajno, F. and Santosh, M.: Rifting, intraplate magmatism, mineral systems and mantle dynamics
875 in central-east Eurasia: An overview, *Ore Geology Reviews*, 63, 265–295,
876 <https://doi.org/10.1016/j.oregeorev.2014.05.014>, 2014.
- 877 Rahman, Md. M. and Ullah, S. E.: Inversion of Gravity Data for Imaging of a Sediment-basement
878 Interface: A Case Study in the Northwestern Part of Bangladesh, *Pure Appl. Geophys.*, 166, 2007–
879 2019, <https://doi.org/10.1007/s00024-009-0530-1>, 2009.
- 880 Rangin, C. and Sibuet, J. C.: Structure of the northern Bay of Bengal offshore Bangladesh:
881 Evidences from new multi-channel seismic data, *Marine and Petroleum Geology*, 84, 64–75,
882 <https://doi.org/10.1016/j.marpetgeo.2017.03.020>, 2017.

- 883 Reimann, K. U. and Hiller, K.: Geology of Bangladesh, 1993.
- 884 Roest, W. R. and Pilkington, M.: Identifying remanent magnetization effects in magnetic data,
885 GEOPHYSICS, 58, 653–659, <https://doi.org/10.1190/1.1443449>, 1993.
- 886 Roy, A. B. and Chatterjee, A.: Tectonic framework and evolutionary history of the Bengal Basin
887 in the Indian subcontinent, *Current Science*, 109, 271–279, 2015.
- 888 Gani, Royhan and Alam, Mustafa: Sedimentation and basin-fill history of the Neogene clastic
889 succession exposed in the southeastern fold belt of the Bengal Basin, Bangladesh: a high-
890 resolution sequence stratigraphic approach, *Sedimentary Geology*, 155, 227–270,
891 [https://doi.org/10.1016/S0037-0738\(02\)00182-3](https://doi.org/10.1016/S0037-0738(02)00182-3), 2003.
- 892 Ruppel, C.: Extensional processes in continental lithosphere, *J. Geophys. Res.*, 100, 24187–24215,
893 <https://doi.org/10.1029/95JB02955>, 1995.
- 894 Smith, W. H. F. and Sandwell, D. T.: Global Sea Floor Topography from Satellite Altimetry and
895 Ship Depth Soundings, *Science*, 277, 1956–1962, <https://doi.org/10.1126/science.277.5334.1956>,
896 1997.
- 897 Sundararajan, N.: A General Perspective on Geophysical Methods in Mineral Exploration, in: On
898 a Sustainable Future of the Earth's Natural Resources, 53–83, 2012.
- 899 Troll, V. R., Mattsson, T., Upton, B. G. J., Emeleus, C. H., Donaldson, C. H., Meyer, R., Weis, F.,
900 Dahrén, B., and Heimdal, T. H.: Fault-Controlled Magma Ascent Recorded in the Central Series
901 of the Rum Layered Intrusion, NW Scotland, *Journal of Petrology*, 61, ega093,
902 <https://doi.org/10.1093/petrology/egaa093>, 2021.
- 903 Uddin, A. and Lundberg, N.: Unroofing history of the eastern Himalaya and the Indo-Burman
904 ranges; heavy-mineral study of Cenozoic sediments from the Bengal Basin, Bangladesh, *Journal*
905 *of Sedimentary Research*, 68, 465–472, <https://doi.org/10.2110/jsr.68.465>, 1998.
- 906 Valdiya, K. S.: *The Making of India*, Springer International Publishing, Cham,
907 <https://doi.org/10.1007/978-3-319-25029-8>, 2016.
- 908 Veevers, J. J.: Gondwanaland from 650–500 Ma assembly through 320 Ma merger in Pangea to
909 185–100 Ma breakup: supercontinental tectonics via stratigraphy and radiometric dating, *Earth-*
910 *Science Reviews*, 68, 1–132, <https://doi.org/10.1016/j.earscirev.2004.05.002>, 2004.
- 911 Zhang, H., Greco, F., Sacek, V., Geng, M., and Liu, P.: Editorial: Applications of gravity
912 anomalies in geophysics, *Front. Earth Sci.*, 12, 1349161,
913 <https://doi.org/10.3389/feart.2024.1349161>, 2024.
- 914 Zhang, S., Li, Z.-X., Evans, D. A. D., Wu, H., Li, H., and Dong, J.: Pre-Rodinia supercontinent
915 Nuna shaping up: A global synthesis with new paleomagnetic results from North China, *Earth and*
916 *Planetary Science Letters*, 353–354, 145–155, <https://doi.org/10.1016/j.epsl.2012.07.034>, 2012.

917 Zhou, M.-F., Robinson, P. T., Leshner, C. M., Keays, R. R., Zhang, C.-J., and Malpas, J.:
918 Geochemistry, Petrogenesis and Metallogenesis of the Panzihua Gabbroic Layered Intrusion and
919 Associated Fe–Ti–V Oxide Deposits, Sichuan Province, SW China, *Journal of Petrology*, 46,
920 2253–2280, <https://doi.org/10.1093/petrology/egi054>, 2005.

921